*Journal of Applied Electrochemistry* **33**: 785–793, 2003.



# The electroformation of Zr metal, Zr–Al alloy and carbon films on ceramic

M. KAWASE[1,2,*] and Y. ITO[2]
[1]*Central Research Institute of Electric Power Industry, 2-6-1 Nagasaka, Yokosuka, Kanagawa, 240-0196 Japan*
[2]*Department of Fundamental Energy Science, Graduate School of Energy Science, Kyoto University, Sakyo-ku, Kyoto 606-8501, Japan*
*(*author for correspondence, e-mail: kawase@criepi.denken.or.jp)*

Received 27 September 2002; accepted in revised form 14 February 2003

*Key words:* carbon film, electrodeposition, molten salt, Zr film, Zr–Al alloy film

**Abstract**

A method of electroforming Zr metal, Zr–Al alloy and carbon film on ceramic substrates has been developed. Using this method, it is possible to apply these films to ceramic substrates, which are complicated in structure. Zr metal and alloy film are formed in the LiCl–KCl melt containing Zr(II), whereas carbon film is formed in the molten carbonate. The electrode consists of a metal part and the ceramic substrate. The films develop between the metal part and the ceramic substrate and propagate along the surface. To form the film there has to be sufficient initial current density to deposit dendritic Zr, carbon whiskers or cubic carbon particles on the metal part.

## 1. Introduction

Ceramic materials coated with metal, which therefore have the advantages of both, metal and ceramic, are used for industrial applications, such as heatproof materials in space stations or ornaments [1, 2]. For the metallization of nonconductive substrates, the following methods can be applied: physical vapour deposition (PVD), chemical vapour deposition (CVD), brazing, electroless plating [3–6]. PVD, CVD and the brazing method are suited for flat and simple shaped substrates, however, they are not suited for complex shaped substrates. Moreover, the electroless plating techniques are hampered by a number of disadvantages including slow and difficult to control rates, high cost and environmental restrictions.

This study focuses on carbon and Zr, of which the electroless deposition is difficult. We have developed an electroforming method using carbon, Zr metal and alloy film on ceramic. This method uses an electrode, which consists of both a metal part and a ceramic part. The metal part is electrodeposited, whereas the ceramic substrate is immediately electroplated in the molten salts.

## 2. Experimental details

### 2.1. *Electroformation of Zr metal and alloy films on ceramic*

Figure 1 shows a schematic diagram of the electrochemical cell. The chamber containing the cell was been specially designed for controlling the atmosphere with optical observation equipment. The electrolyte was a mixture of lithium chloride and potassium chloride (LiCl/KCl = 58.5/41.5 mol %) and was used at 410–550 °C. The gas supplied was Ar. The working electrode consisted of a metal part and the ceramic substrate, as shown in Figure 2. The metal part (Figure 2(a)) has a dimension of 10 mm × 10 mm × 2 mm and the ceramic substrate 10 mm × 50 mm × 2 mm. The cathodic lead was connected to the metal part, which was in contact with the ceramic substrate. Ni, Zr, Ti and Al were used as the metal parts of the working electrode. Alumina ($Al_2O_3$), sapphire ($Al_2O_3$), MgO, BN, Pyrex glass ($SiO_2$/$B_2O_3$/$Al_2O_3$/$Na_2O$ = 80.9/12.7/2.3/4.0) and the single crystal of Si were used as the materials for the ceramic substrate. The counter electrode was a Zr rod, which played a role of supplying the Zr(II) ion by anodic dissolution. Additionally, to supplement the Zr(II) or Zr(IV) ion, a small amount of anhydrous $ZrCl_4$ (0.13 mol %) was added to the electrolyte beforehand. The reference electrode was a silver wire immersed in a LiCl–KCl melt containing 1 mol % of AgCl, which was placed in a glass tube with a thin bottom to maintain the electrical contact with the melt.

### 2.2. *Electroformation of carbon film on ceramic*

A mixture of lithium carbonate and sodium carbonate (Li/Na = 53/47 mol %) was used as the electrolyte. The electrolyte temperature was 650 °C. The gases supplied were mixtures of $H_2$, $CO_2$, $N_2$ and $H_2O$. The metal part of the working electrode was Ni. The material of the

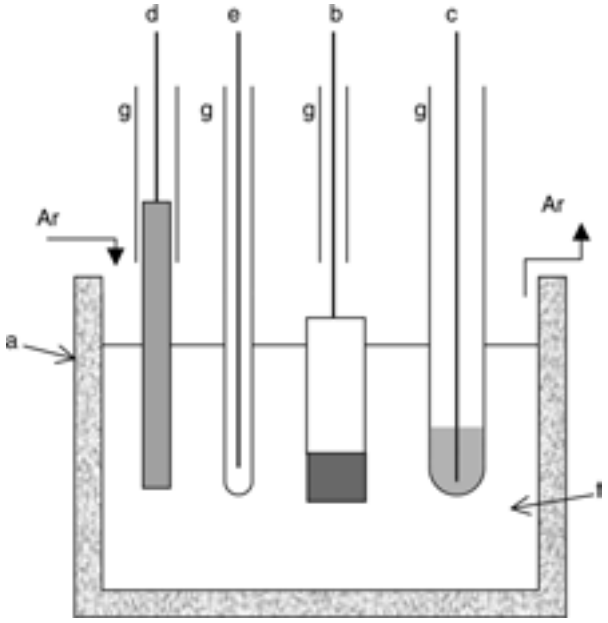


*Fig. 1.* Schematic diagram of the electrochemical cell. Key: (a) alumina crucible, (b) working electrode, (c) reference electrode, (d) counter electrode, (e) thermocouple, (f) electrolyte and (g) alumina tube.

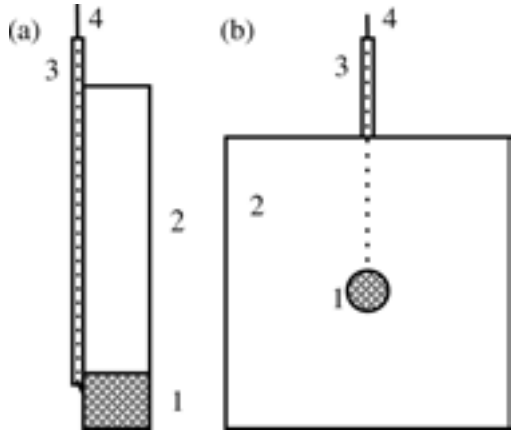


*Fig. 2.* Working electrodes in contact with ceramic. (a) Electrode for electrodeposition; (b) electrode for growth analysis. Key: (1) metal, (2) ceramic, (3) alumina tube and (4) lead.

ceramic substrate was alumina ($Al_2O_3$). The counter electrode was a gold plate (dia. 5 mm, $t = 0.1$ mm). Potentials referred to an Au ($O_2/CO_2 = 33/67\%$) reference electrode.

## 3. Results and discussion

### 3.1. *Zr metal and alloy films on ceramic*

#### 3.1.1. *Cyclic voltammetry*

The following facts have already been established: Zr(II) and Zr(IV) can exist in molten salts between 450 °C and 550 °C, and the ratio of Zr(II) to Zr(IV) depends on the temperature [7, 8]. The ratio (Zr(II)/Zr(IV)) increases with increasing temperature.

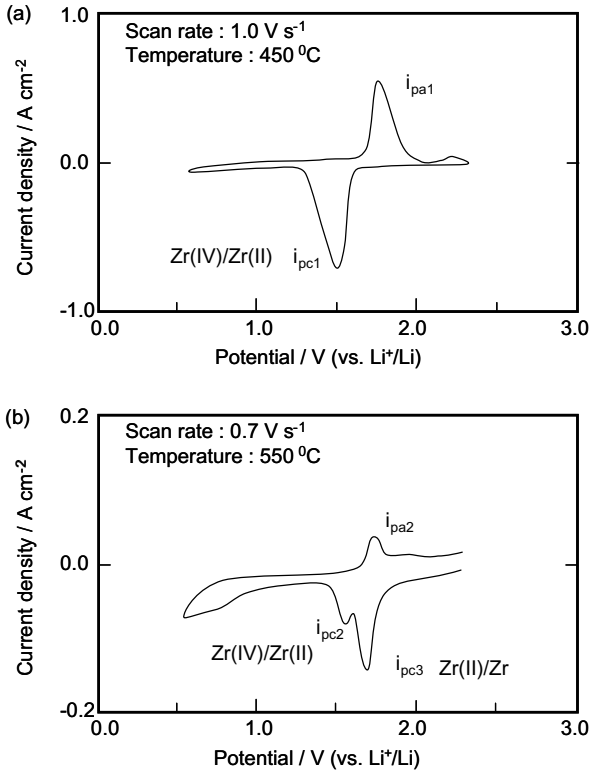


*Fig. 3.* Cyclic voltammograms for anodically dissolved Zr at 450 °C and 550 °C.

In this study, the state of zirconium ions in the electrolyte has also been confirmed by applying a cyclic voltammetry. Cyclic voltammetry was carried out on a Ni electrode after the anodic dissolution of Zr in the LiCl–KCl eutectic. Figure 3(a) and (b) present the cyclic voltammograms at 450 °C and 550 °C. In Figure 3(a), one cathodic peak ($i_{pc1}$) and one anodic peak ($i_{pa1}$) are observed at 1.5 V and 1.8 V vs $Li^+/Li$, respectively. In Figure 3(b), two cathodic peaks ($i_{pc2}$, $i_{pc3}$) and one anodic peak ($i_{pa2}$) are observed at 1.55, 1.7 and 1.8 V, respectively. $i_{pc1}$ and $i_{pc2}$ are related to the reduction of Zr(IV)/Zr(II) according to the following reaction:

$$\mathrm{Zr(IV)} + 2\,\mathrm{e}^- \rightarrow \mathrm{Zr(II)} \quad (1)$$

On the other hand, $i_{pc3}$ is related to the reduction of Zr(II)/Zr according to the following reaction:

$$\mathrm{Zr(II)} + 2\,\mathrm{e}^- \rightarrow \mathrm{Zr} \quad (2)$$

At 450 °C, the concentration of Zr(II) in the electrolyte is low because the peak, which corresponds to $i_{pc3}$, cannot be observed in Figure 3(a). However, at 550 °C, the concentration of Zr(II) in the electrolyte is high, because $i_{pc3}$ is much larger than $i_{pc2}$ as shown in Figure 3(b). Moreover, when the Zr film is formed on a certain metal by electrodeposition, it is noted that the higher the concentration of Zr ion of low valence in the electrolyte, the higher the crystallization and adhesion of the film [9].

Therefore, the electrodeposition at 550 °C is more advantageous than that at 450 °C. Further, the concentration of Zr(IV) decreases with time, because the vaporization of $ZrCl_4$ is high. Hence, the electrodeposition at 450 °C has more disadvantages. Furthermore, the vapourization of the electrolyte becomes higher at over 550 °C. Consequently, the suitable temperature condition of the electrodeposition is approximately between 500 and 550 °C.

### 3.1.2. *Electroformation of Zr metal and alloy film on ceramic*

When the metal part of the working electrode is made of either Zr, Ni, Ti or Fe, a dense Zr film forms on the ceramic. However, when the metal part of the working electrode is made of Al, Zr–Al alloy films in which the concentrations of Al are under 55 at % are formed on the ceramic. These films develop at the edge of the cathodically polarized metal part and propagate along the surface, as shown in Figure 4.

### 3.1.3. *Effect of initial current density*

Table 1 lists the effects of the initial current density of the Zr metal film and the alloy film formations on the alumina substrate. The initial current density was calculated for the surface of the metal part of the working electrode. When the metal part of the working electrode is Zr, the initial current density should be set between 2.0 and 12 mA $cm^{-2}$ to form a good adhesive and homogeneous film. Figure 5(a) and (b) show the SEM image of the Zr film on the alumina substrate under this condition. The adhesion failure load of the film (measured by the scratch test [10]) is about 50 mN. The morphology of the Zr film is prismatic. If the initial current density is set below 2.0 mA $cm^{-2}$, Zr is only deposited on the metal part of the working electrode and a Zr film does not form on the alumina. If the initial current density is set over 12 mA $cm^{-2}$, a film is formed, which is neither adhesive nor homogeneous and peels off easily.

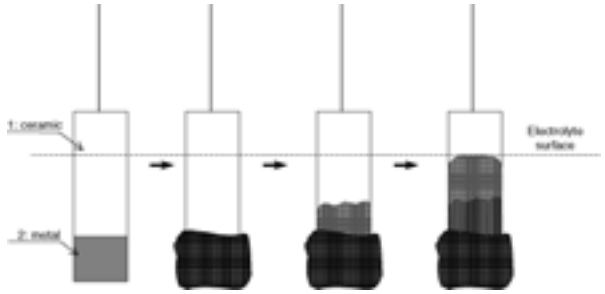

*Fig. 4.* Formation process of Zr film on ceramic.

Further, when the metal part of the working electrode is Ni, Ti or Fe, these conditions of Zr film formation and the morphology of Zr film are much the same as when the metal part is Zr.

However, when the metal part is Al, the conditions of film formation and the film morphology are different from the case when the metal part is Zr. The initial current density should be set between 5.5 and 9.0 mA $cm^{-2}$ to form a good adhesive and homogeneous film. Figure 5(c) and (d) show the SEM-image of the Zr–Al alloy film on the alumina substrate after the potentiostatic electrolysis has been conducted at 1.2 V vs $Li/Li^+$ for 17 h. The initial current density was 9.0 mA $cm^{-2}$. The morphology of the Zr–Al alloy film appears as an aggregation of spherical particles of diameter of 2–5 $\mu$m. The composition of the Zr–Al alloy is 45.1 at % of Zr and 54.9 at % of Al. The morphology and composition of the Zr–Al alloy depend on the current density and temperature. As the concentration of Zr in the Zr–Al alloy film increases, the size of the spherical particles decreases, and the shape of the particles becomes prismatic. The source of Al in the Zr–Al alloy film is generated according to the following reaction at the Al electrode:

$$3\ \mathrm{Zr(II)} + 2\ \mathrm{Al} \rightarrow 3\ \mathrm{Zr} + 2\ \mathrm{Al(III)} \qquad (3)$$

Therefore, the Zr–Al alloy film is formed by the coelectrodeposition of Zr(II) and Al(III).

Moreover, the film formation is related to the morphology of the Zr deposited on the metal part of the working electrode. For example, if the metal part of the working electrode is Zr and the initial current

*Table 1.* Effects of initial current density on Zr metal and alloy film formations on alumina substrates

| Zr electrode | Initial current density /mA $cm^{-2}$ | | |
|---|---|---|---|
| | ~2.0 | 2.0~12 | 12~ |
| Deposit | little or no deposit | Zr | Zr |
| Homogeneity | – | O | × |
| Adhesiveness | – | O | × |
| Morphology | – | prismatic | prismatic |
| Al electrode | ~5.5 | 5.5~9.0 | 9.0~ |
| Deposit | little or no deposit | Zr–Al | Zr–Al, Zr |
| Homogeneity | – | O | × |
| Adhesiveness | – | O | × |
| Morphology | – | spheric | spheric or prismatic |

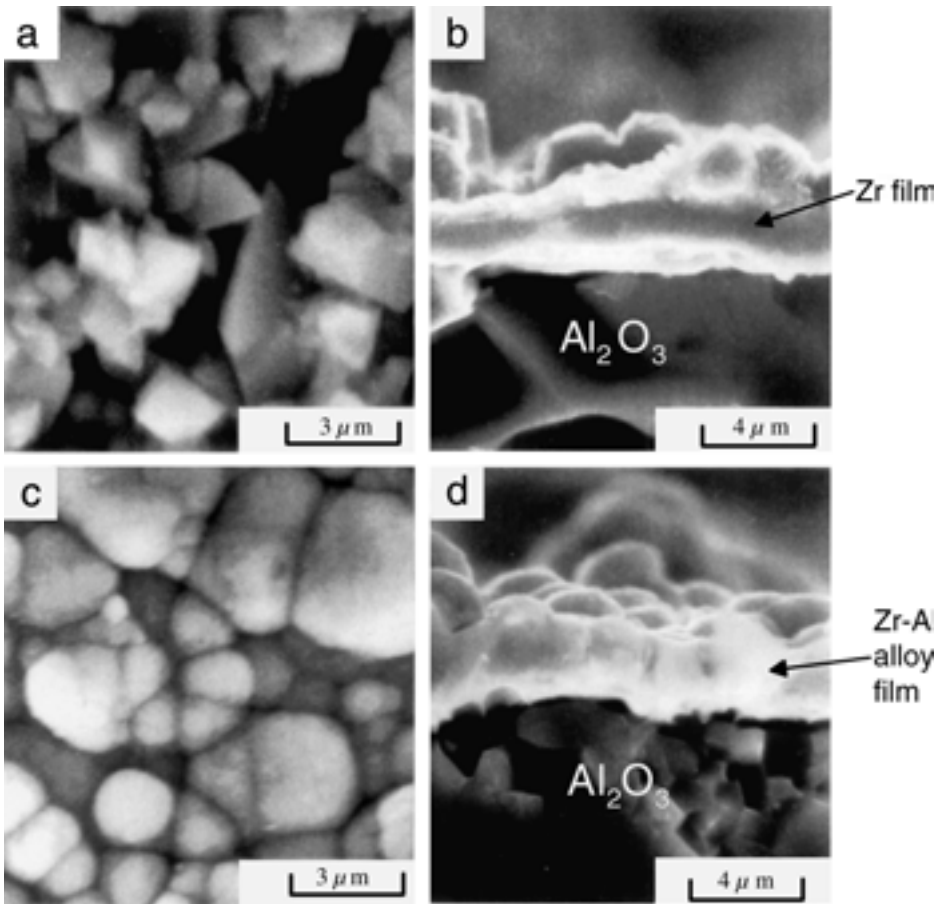


*Fig. 5.* Surface and cross-sectional SEM images of (a)(b) Zr film and (c)(d) Zr–Al alloy film coated on alumina substrates at 530 °C.

density is over 2 mA $cm^{-2}$, which is among the values capable of creating good conditions to form a film on ceramic, Zr is deposited dendritically on the metal part. If the initial current density is under 2 mA $cm^{-2}$, which creates a difficult condition to form a film, Zr is deposited on the metal part; however, the surface of this Zr deposition is not dendritic but nearly smooth. Therefore, in order to form a film on ceramic, sufficient initial current density is necessary to create a dendritic deposition of Zr on the metal part.

3.1.4. *Spreading rate of the film*

To examine the spread rate of the film on ceramic, the films were formed by galvanostatic electrolysis at 1.8 mA (initial current density 9.0 mA $cm^{-2}$). The working electrode is shown in Figure 2(b). The alumina substrate has dimensions 50 mm × 50 mm × 2 mm and a hole of diameter 5 mm in the centre. The metal part, a Zr disc diameter 5 mm × 3 mm, was put into the hole of the alumina substrate. Figure 6 shows the relation between the area the Zr film covers and the electrolysis time. The spread rate of the film is about 2.2 $cm^2$ $h^{-1}$. The current yield of the Zr film formation, which is estimated according to the area and thickness of the film, is approximately 15%. The remaining current yield is used for the Zr deposition on the metal part of the electrode and the Zr film.

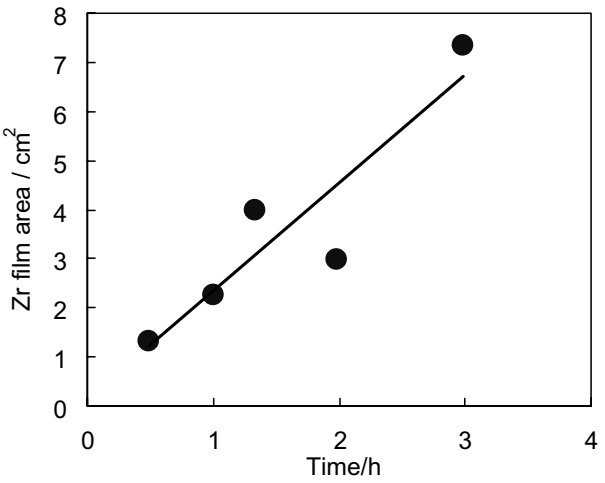


*Fig. 6.* Relationship between the Zr film area and the electrolysis time.

3.1.5. *Other ceramics*

To estimate the effect of the substrate, alumina ($Al_2O_3$), sapphire ($Al_2O_3$(0001)), MgO, BN, Pyrex glass ($SiO_2$/$B_2O_3$/$Al_2O_3$/$Na_2O$ = 80.9/12.7/2.3/4.0) and a single crystal of Si (0 0 1) were used as substrates. The formation of the Zr and Zr–Al alloy film was successful on all substrates. Figure 7 shows the SEM images of the film on each substrate. On the sapphire and Si sub-

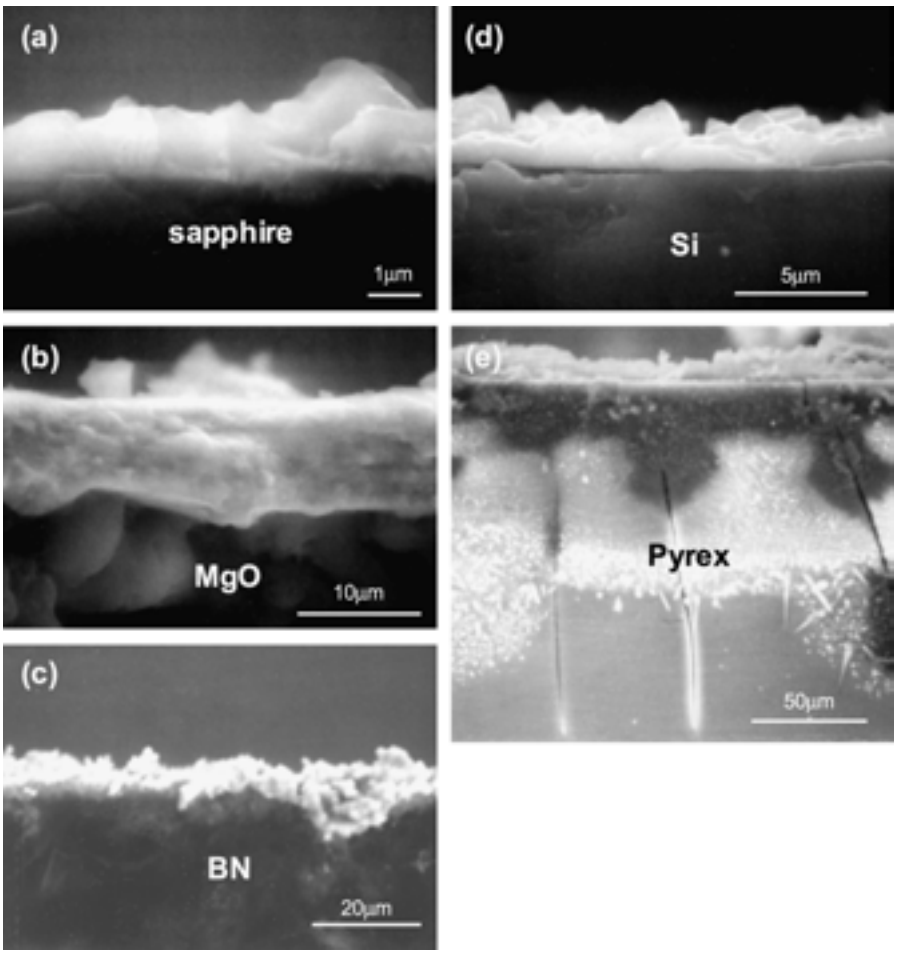


*Fig. 7.* SEM images of the film on other substrates.

strates, the particles constituting the film are smaller and more uniform than those on the alumina substrate. Because the Pyrex glass substrate turns whitish and becomes easier to break by the reaction with the electrolyte, the film is heterogeneous and less adhesive. On the MgO and BN substrates, the films are similar to those on the alumina substrate.

### 3.2. *Carbon film on ceramic*

It is well known that molten carbonate is used as the electrolyte in molten carbonate fuel cells (MCFC). There are many reports which describe the reactions of the electrode in a potential range between 0 V and −1.2 V vs (1:2 $O_2/CO_2$)/Au. However, the potential range suitable for carbon deposition is below −1.4 V, and there are a few reports describing the phenomenon of carbon deposition [11–13].

#### 3.2.1. *Cyclic voltammetry*

Figure 8 presents the cyclic voltammograms in $H_2/CO_2/H_2O = 64/16/20$, $CO_2$ and $N_2$ at 650 °C. All cyclic voltammograms have similar shapes. The cathodic current rises at about −1.4 V. The increase in cathodic current is due to the reduction of $CO_3^{2-}$ according to the following reactions:

$$CO_3^{2-} + 2\,e^- = CO + 2\,O^{2-} \quad (4)$$

$$CO_3^{2-} + 4\,e^- = C + 3\,O^{2-} \quad (5)$$

This cathodic current becomes smaller in the order $H_2/CO_2/H_2O = 64/16/20$, $N_2$ and $CO_2$. Therefore, carbon deposition using $H_2/CO_2/H_2O = 64/16/20$ is easier than when using the other gases. Moreover, the anodic current peak at about −1.2 V is due to the oxidation of the deposited carbon or carbon monoxide.

#### 3.2.2. *Electroformation of carbon film on ceramic*

The carbon film can also be formed on alumina substrates in the same process of Zr film as shown in Figure 4. The film develops between the metal part and the alumina substrate and propagates along the surface. If the carbon film is formed on the alumina, the carbon whiskers or the cubic carbon particles are deposited on the metal part, as shown in Figure 9. Moreover, the carbon whiskers start to form on the carbon-coated alumina closest to the metal part. Therefore, to form the carbon film, it is necessary to deposit the carbon whiskers or the cubic carbon particles on the metal part.

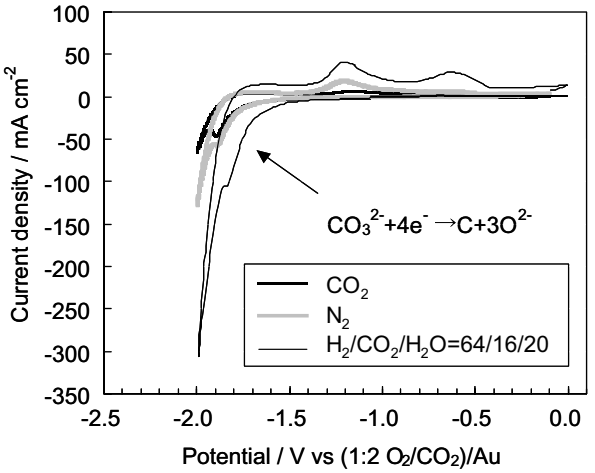


*Fig. 8.* Cyclic voltammograms for Au electrode in $Li_2CO_3$–$Na_2CO_3$ eutectic melt at 650 °C, scan rate 0.1 V $s^{-1}$. Gas compositions are $H_2/CO_2/H_2O = 64/16/20$, $CO_2$ and $N_2$.

3.2.3. *Effects of gas condition on carbon film*

Carbon film can be formed on alumina substrates in $H_2/CO_2/H_2O = 64/16/20$, $CO_2$ and $N_2$. The morphology of the carbon film in $N_2$ is similar to that in $CO_2$. Figure 10 shows the SEM-images of the carbon film in $H_2/CO_2/H_2O = 64/16/20$ and $N_2$. Each film consists of particles. The particles in $H_2/CO_2/H_2O = 64/16/20$ are smaller than those in $N_2$. Moreover, the homogeneity of the film in $H_2/CO_2/H_2O = 64/16/20$ is greater than that in $N_2$.

## 4. Discussion

When the initial current density is larger than a certain critical value, Zr metal, Zr–Al alloy and carbon films are formed on the ceramic substrate. Moreover, the Zr dendrite, the carbon whiskers and the cubic carbon particles are formed on the metal part of the working electrode. It is speculated that the energy required for the formation of the film on ceramic substrates is lower than the energy required for the growth of the dendritic Zr deposition, the carbon whiskers and the cubic carbon particles.

This phenomenon is explained by the classical nucleation theory [14,15]. The total free energy for condensed phase formation, $\Delta G_{net}$, can be calculated theoretically. The value, $\Delta G_{net}$, is the total obtained by adding the free energy of the new phase bulk and its free surface energy:

$$\Delta G_{net} = \Delta G_{bulk} + \Delta G_{surf} \tag{6}$$

If the nucleus is assumed to be a pillar of radius $r$ and height $h$ (Figure 11), Equation 6 can be rewritten as

$$\Delta G_{net} = -\pi r^2 h \frac{\rho n F \eta}{M} + 2\pi r h \gamma \tag{7}$$

where $\rho$ is the density of the deposit, $n$ the number of electrons in the redox reaction, $F$ the faradaic constant, $\eta$ the activation overpotential, $M$ the molecular weight of the deposit, and $\gamma$ is the molar free surface energy (surface tension).

When $\alpha$ metal is deposited on the substrate of $\alpha$ metal, the total free energy is

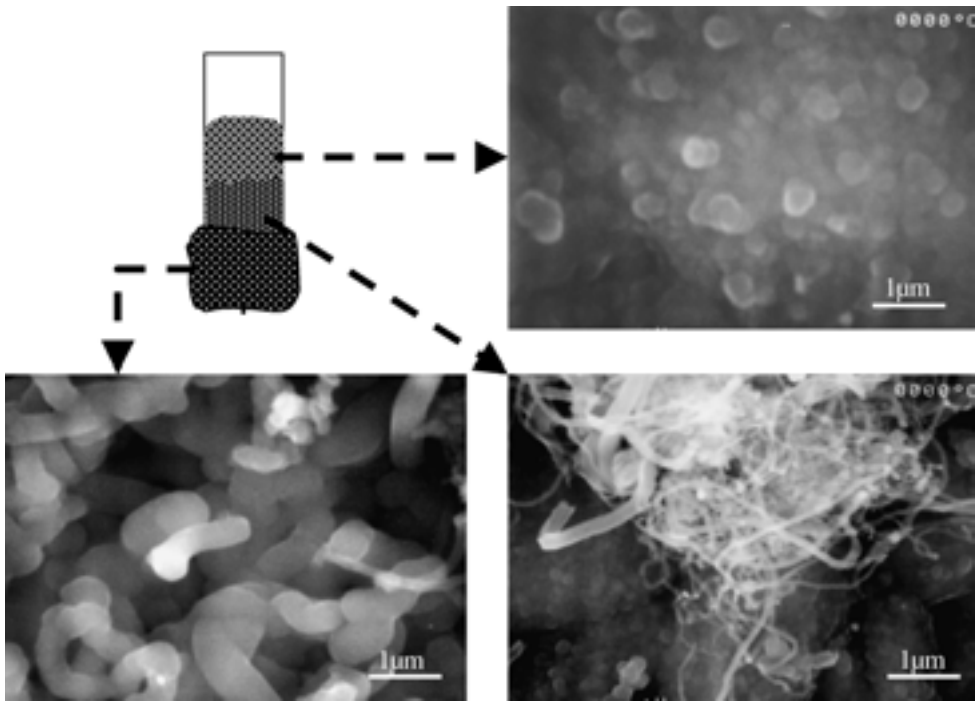


*Fig. 9.* Surface SEM images of the electrode in $H_2/CO_2/H_2O = 64/16/20$.

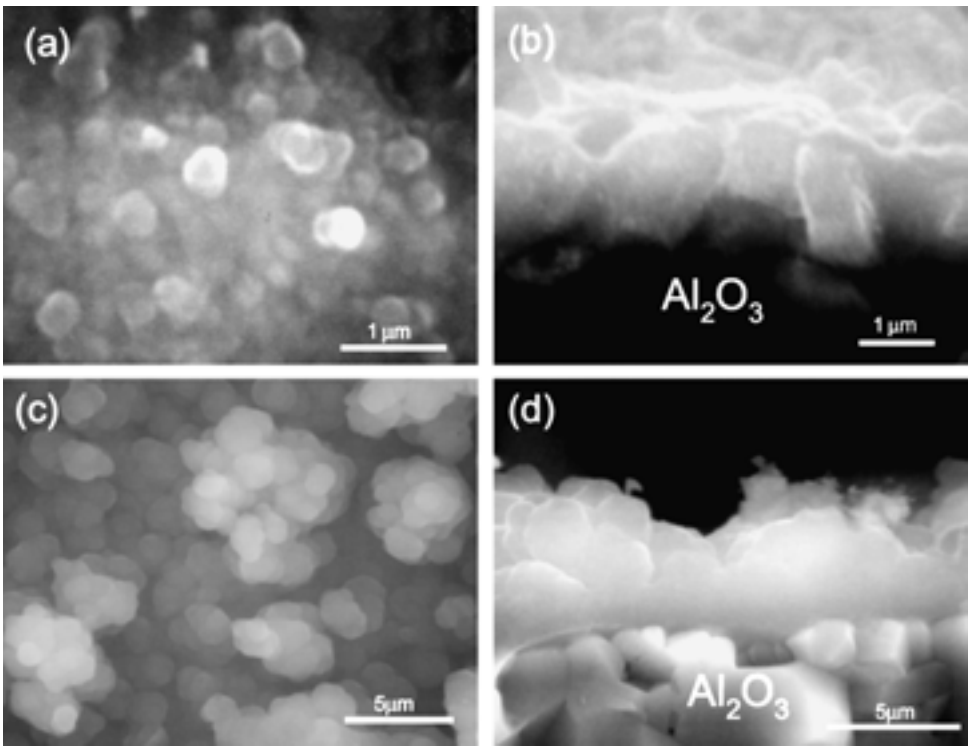


*Fig. 10.* Surface and cross-sectional SEM images of the carbon film in (a)(b) $H_2/CO_2/H_2O = 64/16/20$ and (c)(d) $N_2$.

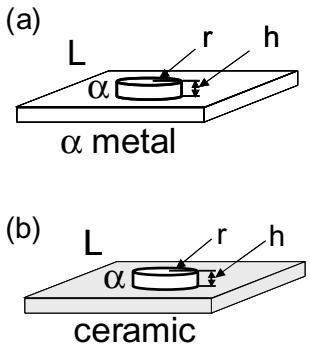


*Fig. 11.* Nucleation on (a) metal and (b) ceramic.

$$\Delta G_\alpha = -\pi r^2 h \frac{\rho_\alpha nF\eta}{M} + 2\pi rh\gamma_{\alpha L} \tag{8}$$

The critical nucleus radius can then be derived and is given by Equation 9. If the nucleus radius is smaller than the critical nucleus radius, the nucleus soon disappears.

$$r^*_\alpha = \frac{M\gamma_{\alpha L}}{\rho_\alpha nF\eta} \tag{9}$$

The critical free energy barrier against nucleation, $\Delta G^*_\alpha$, is determined by substituting $r^*_\alpha$ into Equation 8:

$$\Delta G^*_\alpha = \frac{\pi h(\gamma_{\alpha L})^2 M}{\rho_\alpha nF\eta} = \pi h\gamma_{\alpha L} r^*_\alpha \tag{10}$$

On the other hand, when α metal is deposited on the ceramic substrate, the area ($2\pi rh + \pi r^2$) on the α metal–liquid interface and the area ($\pi r^2$) on the α metal–ceramic interface increase, whereas the area ($\pi r^2$) on the ceramic–liquid interface decreases.

Thus the total free energy is

$$\Delta G_{cera} = -\pi r^2 h \frac{\rho_\alpha nF\eta}{M} + (2\pi rh + \pi r^2)\gamma_{\alpha L} + \pi r^2(\gamma_{\alpha C} - \gamma_C) \tag{11}$$

The critical nucleus radius is given by Equation 12:

$$r^*_{cera} = \frac{\gamma_{\alpha L} h}{\frac{h\rho_\alpha nF\eta}{M} - (\gamma_{\alpha L} + \gamma_{\alpha C} - \gamma_C)} \tag{12}$$

The critical free energy barrier against nucleation, $\Delta G^*_{cera}$, is also determined by inserting $r^*_{cera}$ into Equation 11:

$$\Delta G^*_{cera} = \frac{\pi(h\gamma_{\alpha L})^2}{\frac{h\rho_\alpha nF\eta}{M} - (\gamma_{\alpha L} + \gamma_{\alpha C} - \gamma_C)} = \pi h\gamma_{\alpha L} r^*_{cera} \tag{13}$$

If the nucleation of the α metal on the ceramic substrate is easier than on α metal, the following relation can be determined:

$$\Delta G^*_{cera} < \Delta G^*_\alpha \tag{14}$$

Moreover, the following relations are necessary for setting up Equation 14:

$$\gamma_{\alpha L} + \gamma_{\alpha c} - \gamma_c < 0 \quad (15)$$

or

$$\eta_\alpha < \eta_{cera} \quad (16)$$

If Equation 15 is valid, the film is formed independent of the current density and potential. To form the film, it is not necessary to deposit the α metal dendritic or whiskers on the metal part. Further, the film is formed from the early stages of electrodeposition. However, these phenomena do not take place in practice. Therefore, film formation on ceramic cannot be explained by Equation 15.

On the other hand, because the film formation is dependent on the initial current density (as listed in Table 1), Equation 16 can explain the film formation in the following way using Figure 12 which shows a schematic diagram of the free energy curve deriving from the nucleation. During the early stages of electrodepositing, the overpotential on the surface of the metal part ($\eta_\alpha$) is almost equal to that at the contact point between the metal part and the ceramic substrate ($\eta_{cera}$). In Figure 12, the free energy curves of $\Delta G_\alpha$ and $\Delta G_{cera}$ are shown as curves 1 and 2, respectively. Because $\Delta G_\alpha(\eta_\alpha = \eta_{cera})$ is lower than $\Delta G_{cera}$, the deposition of α metal on the metal part is easier than that on ceramic.

However, as the dendritic α metal deposition grows, the length of a dendrite increases and the ratio of the length to the thickness of the dendrite becomes larger. Therefore, the electric resistance between the metal part of the electrode and the top of the dendrite increases and the overpotential on the dendrite decreases. Hence, the direction sign of inequality in overpotential changes to $\eta_\alpha < \eta_{cera}$ (Equation 16). Under these conditions, $\Delta G^*_{cera}$ is smaller than $\Delta G^*_\alpha$ as shown by curves 2 and 3 in Figure 12 and the nucleation of the α metal occurs on the ceramic. Moreover, the position of the dendritic deposition moves from the metal part of the electrode to the coated part on the ceramic and the film continuously propagates along the surface.

## 5. Conclusion

A method of forming Zr metal, Zr–Al alloy and carbon film on ceramic substrates has been developed. It is possible to produce Zr metal and Zr–Al alloy films in a LiCl–KCl melt containing Zr(II), whereas carbon film is formed in the molten carbonate. For this method, an electrode consisting of a metal part and a ceramic substrate is used. The films develop between the metal part and the ceramic substrate and propagate along the surface. In order to form a film on ceramic substrates, sufficient initial current density is required to deposit dendritic Zr, carbon whiskers or cubic carbon particles on the metal part.

Using this method of film formation, it is possible to coat ceramic substrates, which have complicated struc-

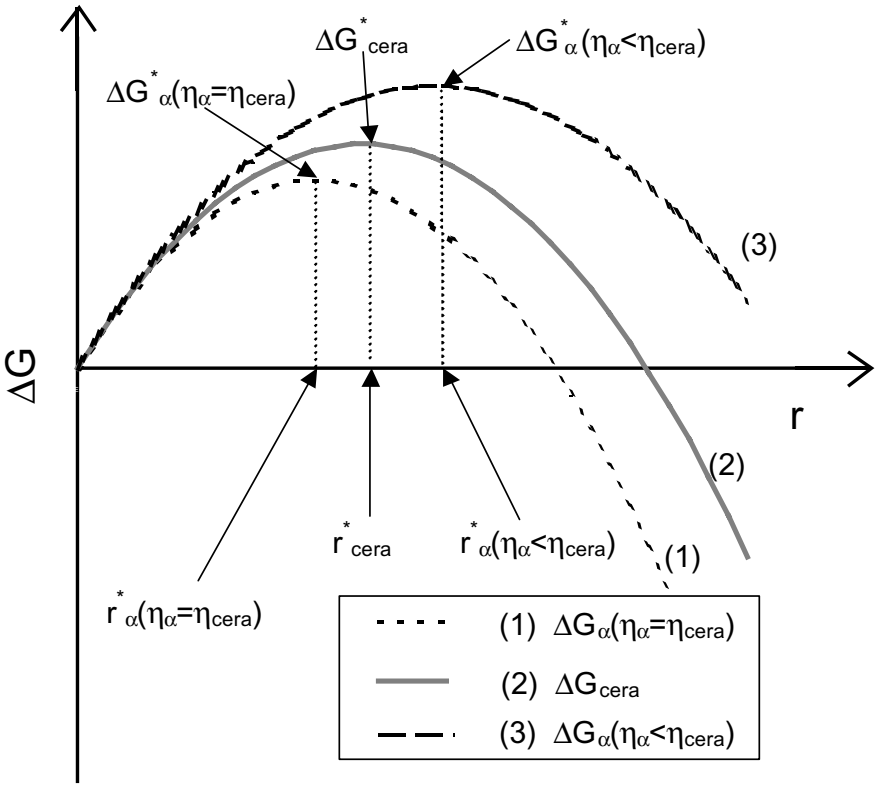


*Fig. 12.* Schematic diagram of the total free energy as a function of the radius of a nucleus.

tures. Moreover, this method suggests that ceramic substrates can be coated with other metals when using appropriate baths.

## References


1. A. Gukelberger and S. Steeb, *Z. Metallkunde*. **69** (1978) 385.
2. D. Weng and U. Landau, *J. Electrochem. Soc*. **142** (1995) 2598.
3. Y. Kato, N. Sugimoto and F. Moriyama, *Kinzoku* **6** (1986) 71.
4. T. Osaka, I. Koiwa, M. Usuda, K. Arai and I. Saito, *J. Electrochem. Soc*. **136** (1989) 1124.
5. T. Oki and J. Tanigawa, *Molten Salts* **25** (1982) 115.
6. S. Yoshida, 'Hakumaku' (Baihukan Co., Tokyo, 1990), p. 16.
7. R. Baboian, D.L. Hill and R.A. Bailey, *J. Electrochem. Soc*. **112** (1965) 1221.
8. T. Suzuki, *Denki Kagaku* **39** (1971) 864.
9. T. Sakakura, *Denki Kagaku* **34** (1966) 780.
10. S. Baba, A. Kikuchi and A. Kinbara, *J. Vac. Sci. Techol*. **A5**(4) (1987) 1860.
11. M.D. Ingram, B. Baron and G.J. Janz, *Electrochim. Acta*. **11** (1966) 1629.
12. J. Dubois, *Ann. Chim., Sci. Mater*. **10** (1965) 145.
13. H.E. Bartlett and K.E. Johson, *J. Electrochem. Soc*. **114** (1967) 457.
14. M. Volmer and A. Weber, *Z. Phys. Chem*. **119** (1926) 227.
15. T. Erdey-Gruz and M. Volmer, *Z. Phys. Chem*. **157** (1931) 165.